

## Effect of the thickness of BiFeO<sub>3</sub> layers on the magnetic and electric properties of BiFeO<sub>3</sub>/La<sub>0.7</sub>Sr<sub>0.3</sub>MnO<sub>3</sub> heterostructures

Le Wang, Zhen Wang, Kui-juan Jin, Jian-qi Li, Huai-xin Yang et al.

Citation: *Appl. Phys. Lett.* **102**, 242902 (2013); doi: 10.1063/1.4811439

View online: <http://dx.doi.org/10.1063/1.4811439>

View Table of Contents: <http://apl.aip.org/resource/1/APPLAB/v102/i24>

Published by the [AIP Publishing LLC](#).

---

### Additional information on *Appl. Phys. Lett.*

Journal Homepage: <http://apl.aip.org/>

Journal Information: [http://apl.aip.org/about/about\\_the\\_journal](http://apl.aip.org/about/about_the_journal)

Top downloads: [http://apl.aip.org/features/most\\_downloaded](http://apl.aip.org/features/most_downloaded)

Information for Authors: <http://apl.aip.org/authors>

## ADVERTISEMENT

### High-Voltage Amplifiers

Voltage Range from  $\pm 50\text{V}$  to  $\pm 60\text{kV}$   
Current to 25A

### Electrostatic Voltmeters

Contacting & Non-Contacting  
Measure to 20kV - Sensitive to 1mV



ENABLING RESEARCH AND  
INNOVATION IN DIELECTRICS,  
ELECTROSTATICS, MATERIALS,  
PLASMAS AND PIEZOS



[www.trekinc.com](http://www.trekinc.com)

## Effect of the thickness of BiFeO<sub>3</sub> layers on the magnetic and electric properties of BiFeO<sub>3</sub>/La<sub>0.7</sub>Sr<sub>0.3</sub>MnO<sub>3</sub> heterostructures

Le Wang, Zhen Wang, Kui-juan Jin,<sup>a)</sup> Jian-qi Li, Huai-xin Yang, Can Wang, Rui-qiang Zhao, Hui-bin Lu, Hai-zhong Guo, and Guo-zhen Yang

Beijing National Laboratory for Condensed Matter Physics, Institute of Physics, Chinese Academy of Sciences, Beijing 100190, China

(Received 1 May 2013; accepted 2 June 2013; published online 17 June 2013)

BiFeO<sub>3</sub> layers with various thicknesses were fabricated on La<sub>0.7</sub>Sr<sub>0.3</sub>MnO<sub>3</sub> covered SrTiO<sub>3</sub> substrates by a laser molecular-beam epitaxy system. The ferromagnetic transition temperature ( $T_c$ ) and magnetic coercive field ( $H_c$ ) of BiFeO<sub>3</sub>/La<sub>0.7</sub>Sr<sub>0.3</sub>MnO<sub>3</sub> heterostructures are larger than those of the La<sub>0.7</sub>Sr<sub>0.3</sub>MnO<sub>3</sub> film. With increasing the thickness of the BiFeO<sub>3</sub> layer,  $T_c$ ,  $H_c$ , and ferroelectric coercive field of the BiFeO<sub>3</sub>/La<sub>0.7</sub>Sr<sub>0.3</sub>MnO<sub>3</sub> heterostructures decrease, while the dielectric permittivity, remanent polarization, and resistance ratio of the ON and OFF states increase. The variations of the magnetic and electric properties with the thickness could be due to the effects of the epitaxial strain and the interface layer. © 2013 AIP Publishing LLC.

[<http://dx.doi.org/10.1063/1.4811439>]

Multiferroic materials, which combine multiple order parameters, provide a great opportunity to couple phenomena such as electronic and magnetic order.<sup>1–4</sup> Among these materials, perovskite-structure BiFeO<sub>3</sub> (BFO) has currently attracted a lot of attention because of its large polarization, high Curie temperature ( $\sim 1100$  K), and high Neel temperature ( $\sim 643$  K). La<sub>0.7</sub>Sr<sub>0.3</sub>MnO<sub>3</sub> (LSMO) is a ferromagnetic material at room temperature and compatible with ferroelectric BFO in crystal structure. Therefore, it is interesting to combine these two materials to form a ferroelectric-ferromagnetic heterostructure, which will open the perspective of combining multiple degrees of freedom to design a multifunctional device. Recently, many researchers have made efforts to study the coupling characteristics in BiFeO<sub>3</sub>/La<sub>0.7</sub>Sr<sub>0.3</sub>MnO<sub>3</sub> (BFO/LSMO) heterostructures.<sup>5–9</sup>

Moreover, the variation of the film thickness plays an important role in the physical properties of the film system.<sup>10,11</sup> Different states of compressive or tensile strains can be obtained by changing the thickness of the BFO film.<sup>12</sup> Several studies have been reported that the magnetization of the BFO film decreases with increasing the thickness of the BFO film.<sup>13–15</sup> The possible origins for the thickness-dependent magnetic properties of BFO films were ascribed to the large lattice misfit,<sup>13,14</sup> the surface-to-volume ratio, and the interface layer.<sup>15</sup> However, there are some inconsistent results in some works about the effect of the thickness on the ferroelectric properties of BFO films.<sup>12,16–21</sup> For example, the first-principles study on (111)-oriented BFO films showed that the polarization is almost independence of the film thickness.<sup>17</sup> However, Jang *et al.* have observed that the remanent polarization of high quality (001)-oriented epitaxial BFO films shows strong dependence of the film thickness.<sup>12</sup> Therefore, the effect of the thickness on the ferroelectric properties of BFO films is still needed to be further investigated. In this work, the effect of the thickness on

the magnetic and electrical properties of the BFO/LSMO heterostructures with various BFO thicknesses of 150, 300, 450, and 600 nm has been investigated, and the related mechanisms are discussed by considering the effects of the epitaxial strain and the interfacial layer. These results will provide us some insight into the nature of physical properties of the ferroelectric/ferromagnetic heterostructures.

BFO/LSMO heterostructures (with 120-nm-thick LSMO layer) with various BFO thicknesses of 150, 300, 450, and 600 nm were deposited on (001)-oriented SrTiO<sub>3</sub> (STO) single crystals by a laser molecular-beam epitaxy system (Laser-MBE) at oxygen pressures of 40 Pa for LSMO and 10 Pa for BFO, respectively, using a XeCl 308 nm excimer laser with an energy density of  $\sim 2$  J/cm<sup>2</sup> and a repetition rate of 2 Hz. The temperature of the substrates determined by an infrared pyrometer was kept around 580 °C. After the deposition, the samples were annealed at the same temperature under an oxygen pressure of 3 kPa for 20 min and then cooled down to room temperature. For comparison, a bare LSMO thin film also has been fabricated on the STO substrate. The crystal structure was identified by high-resolution Synchrotron X-ray diffractometry by the BL14B1 beam line of Shanghai Synchrotron Radiation Facility (SSRF), using a 1.24 Å X-rays with a Huber 5021 six-axes diffractometry. The crystalline structure of the BFO/LSMO/STO heterostructure was characterized by transmission electron microscopy (TEM). Magnetic properties of the LSMO thin film and the BFO/LSMO/STO heterostructures were measured with a Quantum Design physical properties measurement system. For electrical measurements, circular Au electrodes with a diameter of 100  $\mu$ m and a thickness of 50 nm were deposited on the surface of the BFO layers. The dielectric properties of the BFO/LSMO/STO heterostructures were measured using an Agilent Impedance Analyzer 4294A at room temperature. The ferroelectric hysteresis loops of the BFO/LSMO/STO heterostructures were measured with a ferroelectric test system (Radiant Technologies) at 20 kHz. The current-voltage curves were measured by using computer-controlled

<sup>a)</sup> Author to whom correspondence should be addressed. Electronic mail: [kjjin@iphy.ac.cn](mailto:kjjin@iphy.ac.cn)

Keithley meters with a delay time of 0.2 s for reading a current value at room temperature. Junction resistances of the BFO/LSMO/STO heterostructures were measured with a high-resistance meter (Keithley 6517).

Large angle x-ray  $\theta - 2\theta$  scans ( $10^\circ$  to  $40^\circ$ ) of the BFO/LSMO/STO heterostructures showed only diffraction peaks from the substrates and (001) reflection peaks for BFO and LSMO, indicating that both the BFO and LSMO layers were free of impurities. Figure 1(a) shows the dependence of the BFO out-of-plane lattice constant ( $c$ ) on the thickness of the BFO layer ( $t_{\text{BFO}}$ ). As  $t_{\text{BFO}}$  increases from 150 to 600 nm, the (002) peak shifts toward the higher angle, indicating the decrease of  $c$ . The variations of the  $c$  values of the BFO and LSMO layers with  $t_{\text{BFO}}$  are presented in Fig. 1(b). The lattice constant for bulk BFO, LSMO, and STO is 3.96 Å,<sup>22</sup> 3.87 Å,<sup>23</sup> and 3.91 Å, respectively. Lattice mismatch between LSMO and STO results in an in-plane tensile strain, causing a compression of the lattice constant in the out-of-plane direction for LSMO layers, as shown in the lower part of Fig. 1(b). On the other hand, the lattice mismatch between BFO and LSMO results in an in-plane compressive strain that causes an elongation of the lattice constant in the out-of-plane direction for BFO layers. This strain gradually decreases with increasing  $t_{\text{BFO}}$ , as shown in the upper part of Fig. 1(b). Therefore, the value of  $c$  of the BFO layer is larger than that of the bulk BFO and decreases from 4.00 to 3.97 Å with  $t_{\text{BFO}}$  increasing from 150 to 600 nm. The cross-sectional TEM images of the BFO/LSMO/STO heterostructure with  $t_{\text{BFO}}$  of 300 nm are shown in Fig. 1(c) for the LSMO/STO interface and in Fig. 1(d) for the BFO/LSMO interface, respectively. The TEM images show that the heterostructure has well-defined interfaces of LSMO/STO and BFO/LSMO and high epitaxial quality of BFO and LSMO

layers. Furthermore, the TEM analysis shows that the in-plane lattice constant is strained to be 3.91 Å for LSMO and 3.92 Å for BFO, which is in agreement with our strain analysis.

The magnetic properties of the LSMO thin films and the BFO/LSMO/STO heterostructures were measured, respectively, with a magnetic field applied along the film plane. The magnetic moment versus temperature ( $M-T$ ) curves after field cooling (FC) were measured at 100 Oe, as shown in Fig. 2(a). Figure 2(b) shows the magnetic hysteresis ( $M-H$ ) loops at 10 K after zero-field cooling. Figure 2(c) shows the BFO layer thickness dependence of the ferromagnetic transition temperature  $T_c$  (calculated value from the Curie-Weiss law  $\chi = \frac{C}{T-T_c}$ , where  $\chi$  is the magnetic susceptibility,  $C$  is a material-specific Curie constant,  $T$  is absolute temperature, and  $T_c$  is the Curie temperature) and the magnetic coercive field  $H_c$  at 10 K. Both values of  $T_c$  and  $H_c$  of BFO/LSMO/STO heterostructures are higher than those of the bare LSMO film without BFO, consistent with previous experimental results.<sup>6,24</sup> This may be due to the exchange coupling at the ferromagnetic-antiferromagnetic interface.<sup>6,25</sup> As a result of this exchange coupling, the ferromagnetic order can be maintained at the temperature above  $T_c$  (325 K) of the bare LSMO film without BFO, which leads to a higher transition temperature and a larger magnetic coercive field for the BFO/LSMO/STO heterostructures. Moreover,  $T_c$  and  $H_c$  values decrease with the increase of  $t_{\text{BFO}}$ , which indicates that this exchange coupling effect may depend on the thickness of the antiferromagnetic layer.<sup>25</sup> More investigations on this matter are still needed.

Figure 3(a) shows the frequency dependence of relative dielectric permittivity ( $\epsilon_r$ ) and dielectric loss of the Au/BFO/LSMO/STO heterostructures with various BFO

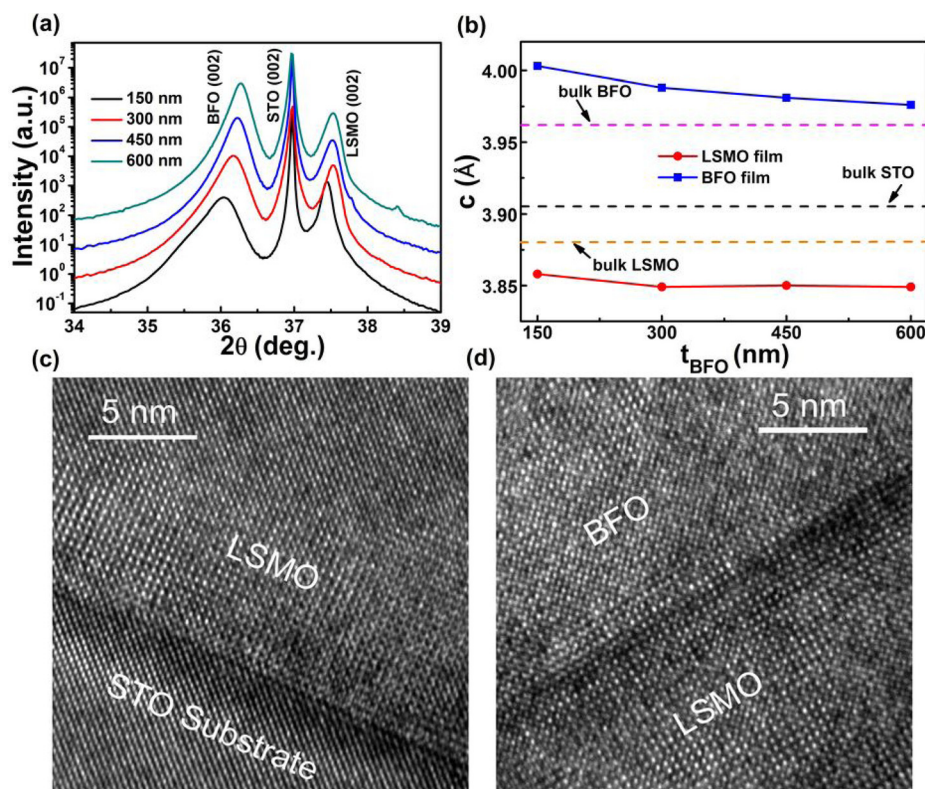


FIG. 1. (a) (002) peaks from x-ray scans showing the effect of  $t_{\text{BFO}}$  on heteroepitaxial strain. (b) Out-of-plane lattice constant as a function of  $t_{\text{BFO}}$ . (c), (d) High-resolution TEM images for the LSMO/STO interface and the BFO/LSMO interface of the BFO/LSMO/STO heterostructure with  $t_{\text{BFO}}$  of 300 nm, respectively.

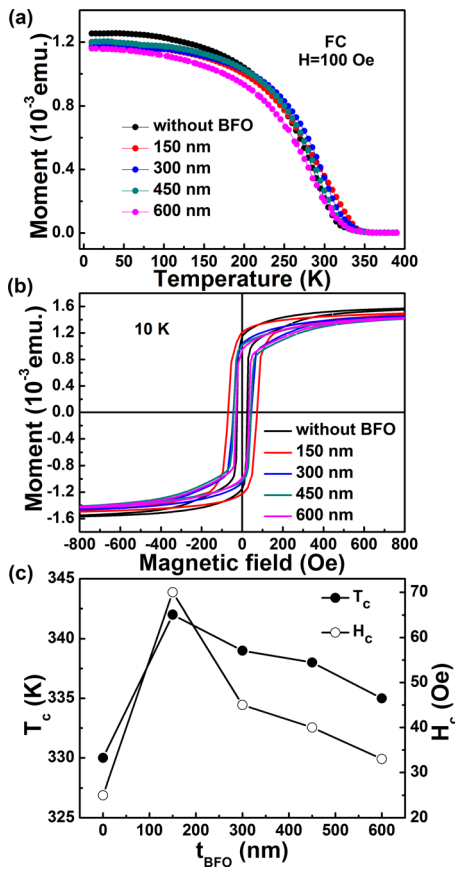


FIG. 2. (a) In-plane field cooling  $M$ - $T$  curves for the LSMO film without BFO and the BFO/LSMO/STO heterostructures with various BFO thicknesses. The cooling and measuring fields are both 100 Oe. (b) The magnetic hysteresis loops of the LSMO film without BFO and the BFO/LSMO/STO heterostructures with various BFO thicknesses at 10 K. (c) BFO layer thickness dependence of  $T_c$  and  $H_c$  at 10 K.

layer thicknesses.  $\epsilon_r$  can be calculated from the measured capacitance using following equation:  $\epsilon_r = \frac{C_p t_{BFO}}{\epsilon_0 A}$ , where  $C_p$  is the measured capacitance,  $\epsilon_0$  is the free space permittivity value, and  $A$  is the capacitor area. It can be found that  $\epsilon_r$  increases, while the dielectric loss decreases with increasing  $t_{BFO}$  in the frequency range of 1 kHz-1 MHz. Moreover, the dielectric loss increases obviously with increasing frequency larger than 100 kHz. Such an increase in dielectric loss should be attributed to the conductor loss contribution of the metallic electrode.<sup>26</sup>

Figure 3(b) shows the variation of  $\epsilon_r$  and dielectric loss with  $t_{BFO}$  measured at 1 MHz. It can be seen that  $\epsilon_r$  increases with increasing  $t_{BFO}$  and then tends to a saturation value. As shown in Fig. 1(b), the epitaxial strain decreases with increasing  $t_{BFO}$ . The reduction of the strain in thicker BFO layers decreases the substrate clamping, and may favor forming the 180° domains and further increasing the dielectric permittivity. Therefore, the variation of the strain with  $t_{BFO}$  could affect the dielectric permittivity of ferroelectric films. The thickness dependence of  $\epsilon_r$  should also be related to the interfacial layer between the films and electrode, which has a low dielectric permittivity and can reduce the effective permittivity of the film due to series connection with the actual dielectric layer.<sup>27</sup> Thus, the effect of the interfacial layer on the  $\epsilon_r$  can be more obvious for the thinner BFO layers. In addition, the dielectric loss decreases from 0.11 to 0.02 when

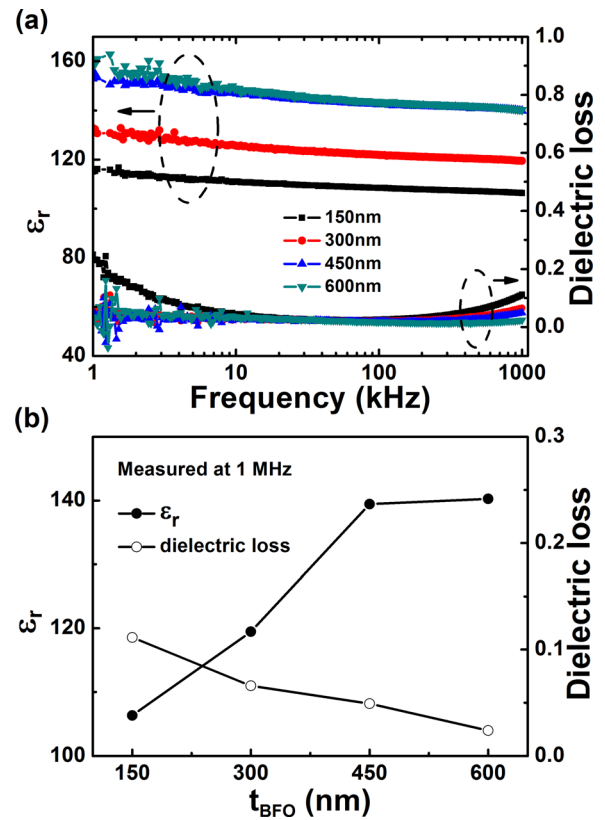


FIG. 3. (a) Frequency dependence of  $\epsilon_r$  and dielectric loss of Au/BFO/LSMO/STO heterostructures with various BFO thicknesses at the room temperature. (b) BFO layer thickness dependence of  $\epsilon_r$  and dielectric loss.

$t_{BFO}$  increases from 150 to 600 nm. The reason for the larger dielectric loss in the thinner BFO layer may be due to the higher leakage current.<sup>28</sup>

Figure 4(a) shows the ferroelectric hysteresis loops ( $P$ - $E$  loops) of the Au/BFO/LSMO/STO heterostructures with various BFO layer thicknesses at room temperature. All the samples exhibit good  $P$ - $E$  loops. The ferroelectric coercive field  $E_c^*$  (defined as  $E_c^* = (+E_c - (-E_c))/2$ ) and remanent polarization  $P_r^*$  (defined as  $P_r^* = (+P_r - (-P_r))/2$ ) as a function of  $t_{BFO}$  are shown in Fig. 4(b). It can be seen that  $E_c^*$  decreases with increasing  $t_{BFO}$ . In general, the reduction of the epitaxial strain, the effect of the interfacial layer, and the pinning of the domain wall will induce the decrease in  $E_c^*$  in the thicker films.<sup>27,29,30</sup> On the other hand, the  $P_r^*$  of the Au/BFO/LSMO/STO heterostructure increases from 57, 80, 98 to 101  $\mu\text{C}/\text{cm}^2$  with increasing  $t_{BFO}$  from 150, 300, 450 to 600 nm, respectively. This large enhancement of  $P_r^*$  is related to the strain relaxation, which is in agreement with that reported in Ref. 20 and is consistent with the fact that the epitaxial strain decreases with the increase of  $t_{BFO}$  shown in Fig. 1(b).

Figure 5(a) shows the current-voltage ( $I$ - $V$ ) characteristics of the Au/BFO/LSMO/STO heterostructures with various BFO layer thicknesses at room temperature. The numbers in the figure denote the sequence of voltage sweeps. Distinct  $I$ - $V$  hysteresis behaviors were observed and reproducible, indicating typical nonvolatile resistive switching behaviors. Figure 5(b) shows the  $I$ - $V$  curves plotted on semilogarithmic scales. From Fig. 5(b), it can be seen that the ON/OFF-state resistance ratio (defined as  $R_{\text{high}}/R_{\text{low}}$ , where  $R_{\text{high}}$  is the high

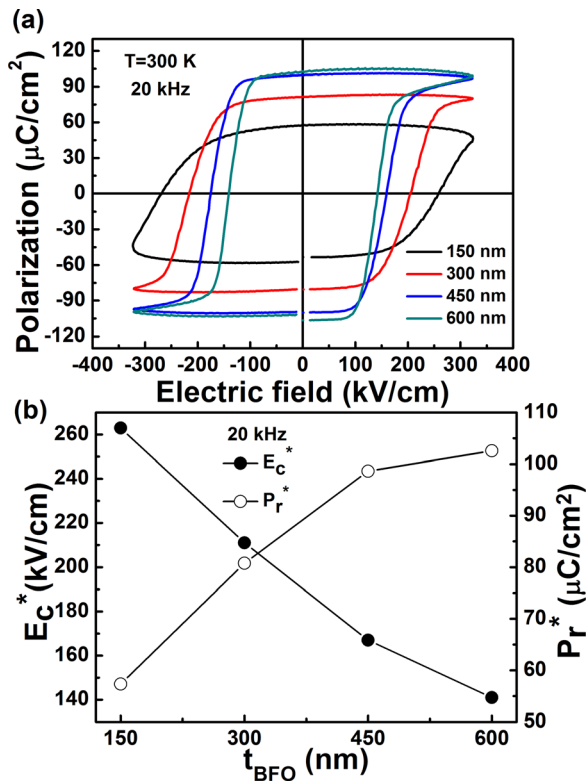


FIG. 4. (a)  $P$ - $E$  loops of Au/BFO/LSMO/STO heterostructures with various BFO thicknesses at the room temperature. The test frequency is 20 kHz. (b) BFO layer thickness dependence of  $E_c^*$  and  $P_r^*$ .

resistance state and  $R_{low}$  is the low resistance state) of the Au/BFO/LSMO/STO heterostructure decreases with decreasing  $t_{BFO}$  at the same read voltage ( $V_{read}$ ). In a ferroelectric

capacitance structure, the metal-ferroelectric interfaces at the top and bottom electrodes would influence the conduction of the heterostructures due to the Schottky barriers. In our previous work, we have analyzed the potential barriers and their variation with ferroelectric switching, and concluded that the origin of the resistive switching effect is due to the polarization-modulated Schottky-like barriers.<sup>31,32</sup> Switching the polarization by changing the polarity of the pulse voltage will result in two different barrier heights and thus two different resistance states. Therefore, the thickness-dependent ON/OFF-state resistance ratio can be attributed to the thickness issue of the polarization shown in Fig. 4(b). Figure 5(c) shows the variations of the junction resistance of the Au/BFO/LSMO/STO heterostructure with  $t_{BFO}$  of 600 nm with a train of +18 V and -18 V pulse voltage. It can be seen that the junction resistance switches from  $R_{high}$  to  $R_{low}$  by changing the polarity of the pulse voltage. The ON/OFF-state resistance ratio of the Au/BFO/LSMO/STO heterostructure with  $t_{BFO}$  of 600 nm is about  $10^3$  at -2 V. The repetition characteristic of the Au/BFO/LSMO/STO heterostructure with  $t_{BFO}$  of 600 nm is shown in Fig. 5(d). No significant changes in the junction resistance for  $2 \times 10^4$  s were observed, indicating that the Au/BFO/LSMO/STO heterostructures are stable at room temperature.

Overall, the effects of the strain and the interfacial layer between BFO and LSMO play the dominant roles in the properties of the BFO/LSMO/STO heterostructure. The epitaxial strain decreases with increasing  $t_{BFO}$ , and the reduction of the strain in thicker BFO layers decreases the substrate clamping, which may favor forming the  $180^\circ$  domains and further increasing  $\epsilon_r$  and  $P_r^*$ . The increase of

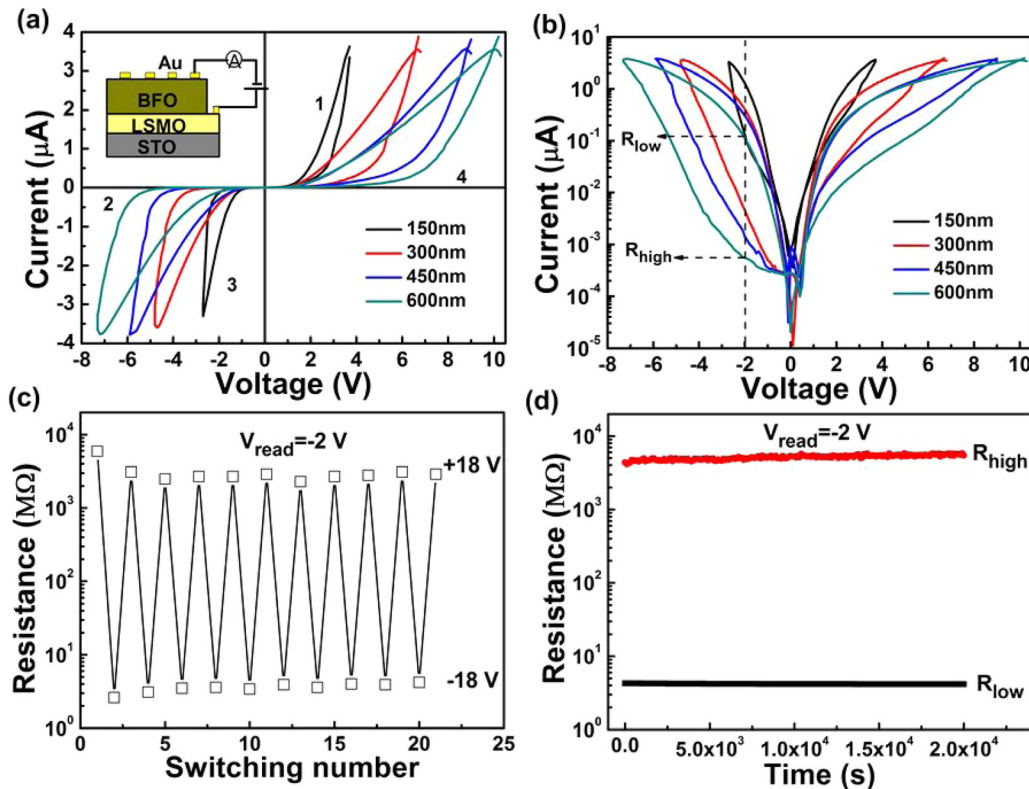


FIG. 5. (a)  $I$ - $V$  curves of Au/BFO/LSMO/STO heterostructures with various BFO thicknesses at the room temperature. (b)  $I$ - $V$  curves plotted on semilogarithmic scales. (c) The  $R_{high}$  and  $R_{low}$  of the Au/BFO/LSMO/STO heterostructure with  $t_{BFO}$  of 600 nm with repetition of polarization-orientation switching. (d) The repetition characteristics of the  $R_{high}$  and  $R_{low}$  of the Au/BFO/LSMO/STO heterostructure with  $t_{BFO}$  of 600 nm.

the value of  $P_r^*$  in thicker BFO layers contributes to the increase of the ON/OFF-state resistance ratio. Moreover, the dielectric loss decreases with increasing  $t_{BFO}$ , which means that the domain wall motion becomes easier.<sup>27</sup> Therefore, smaller electric fields can accomplish the domain wall motion, and the smaller  $E_c^*$  in thicker BFO layers are observed, similar results were also demonstrated by other groups.<sup>29,30</sup> On the other hand, the interfacial layer with smaller dielectric permittivity can cause a noticeable decrease in  $\epsilon_r$  of the thinner BFO layers, while such effect decreases with increasing  $t_{BFO}$ . And the exchange coupling effect at the ferromagnetic-antiferromagnetic interface may be also related to the effect of the interfacial layer, which affects the magnetic properties of the Au/BFO/LSMO/STO heterostructure.<sup>25</sup> Therefore, the improvement of the Au/BFO/LSMO/STO heterostructure performance can be realized by selecting an appropriate thickness of the BFO layer.

In conclusion, BFO layers with various thicknesses from 150 to 600 nm have been fabricated on LSMO-covered (001)-oriented STO single crystals by Laser-MBE. Both values of  $T_c$  and  $H_c$  of BFO/LSMO/STO heterostructures are larger than those of the bare LSMO film and decrease with increasing  $t_{BFO}$ . On the other hand, the dielectric, ferroelectric, and resistive switching characteristics of Au/BFO/LSMO/STO heterostructures are gradually improved with increasing  $t_{BFO}$  and tend to be saturated when  $t_{BFO}$  is larger than 450 nm. The Au/BFO/LSMO/STO heterostructure with  $t_{BFO}$  of 600 nm possesses a large  $P_r^*$  ( $\sim 100 \mu\text{C}/\text{cm}^2$ ) and a high ON/OFF-state resistance ratio ( $\sim 10^3$ ), which can be useful for further application in ferroelectric resistive random-access memories.

This work was supported by the National Basic Research Program of China (Nos. 2012CB921403 and 2013CB328706) and the National Natural Science Foundation of China (Nos. 11134012 and 11174355). The authors wish to thank the Shanghai Synchrotron Radiation Facility (SSRF) for the help in the measurement of XRD.

<sup>1</sup>W. Känzig, *Ferroelectrics and Antiferroelectrics in Solid State Physics* (Academic, New York, 1957), Vol. 4, pp. 5–6.

<sup>2</sup>T. Kimura, T. Goto, H. Shintani, K. Ishizaka, T. Arima, and Y. Tokura, *Nature (London)* **426**, 55 (2003).

<sup>3</sup>N. Hur, S. Park, P. A. Sharma, J. S. Ahn, S. Guha, and S.-W. Cheong, *Nature (London)* **429**, 392 (2004).

<sup>4</sup>W. Eerenstein, N. D. Mathur, and J. F. Scott, *Nature (London)* **442**, 759 (2006).

<sup>5</sup>H. Béa, M. Gajek, M. Bibes, and A. Barthélémy, *J. Phys.: Condens. Matter* **20**, 434221 (2008).

<sup>6</sup>L. You, C. L. Lu, P. Yang, G. C. Han, T. Wu, U. Luders, W. Prellier, K. Yao, L. Chen, and J. L. Wang, *Adv. Mater.* **22**, 4964 (2010).

<sup>7</sup>P. Yu, J. S. Lee, S. Okamoto, M. D. Rossell, M. Huijben, C. H. Yang, Q. He, J. X. Zhang, S. Y. Yang, M. J. Lee, Q. M. Ramasse, R. Erni, Y. H. Chu, D. A. Arena, C. C. Kao, L. W. Martin, and R. Ramesh, *Phys. Rev. Lett.* **105**, 027201 (2010).

<sup>8</sup>C. T. Nelson, P. Gao, J. R. Jokisaari, C. Heikes, C. Adamo, A. Melville, S. H. Baek, C. M. Folkman, B. Winchester, Y. J. Gu, Y. M. Liu, K. Zhang, E. G. Wang, J. Y. Li, L. Q. Chen, C. B. Eom, D. G. Schlom, and X. Q. Pan, *Science* **334**, 968 (2011).

<sup>9</sup>M. J. Calderon, S. Liang, R. Yu, J. Salafranca, S. Dong, S. Yunoki, L. Brey, A. Moreo, and E. Dagotto, *Phys. Rev. B* **84**, 024422 (2011).

<sup>10</sup>J. Wang, J. B. Neaton, H. Zheng, V. Nagarajan, S. B. Ogale, B. Liu, D. Viehland, V. Vaithyanathan, D. G. Schlom, U. V. Waghmare, N. A. Spaldin, K. M. Rabe, M. Wuttig, and R. Ramesh, *Science* **299**, 1719 (2003).

<sup>11</sup>C. Adamo, X. Ke, H. Q. Wang, H. L. Xin, T. Heeg, M. E. Hawley, W. Zander, J. Schubert, P. Schiffer, D. A. Muller, L. Maritato, and D. G. Schlom, *Appl. Phys. Lett.* **95**, 112504 (2009).

<sup>12</sup>H. W. Jang, S. H. Baek, D. Ortiz, C. M. Folkman, R. R. Das, Y. H. Chu, P. Shafer, J. X. Zhang, S. Choudhury, V. Vaithyanathan, Y. B. Chen, D. A. Felker, M. D. Biegalski, M. S. Rzchowski, X. Q. Pan, D. G. Schlom, L. Q. Chen, R. Ramesh, and C. B. Eom, *Phys. Rev. Lett.* **101**, 107602 (2008).

<sup>13</sup>D. S. Rana, K. Takahashi, K. R. Mavani, I. Kawayama, H. Murakami, M. Tonouchi, T. Yanagida, H. Tanaka, and T. Kawai, *Phys. Rev. B* **75**, 060405(R) (2007).

<sup>14</sup>Y. Wang, Y. H. Lin, and C. W. Nan, *J. Appl. Phys.* **104**, 123912 (2008).

<sup>15</sup>F. Z. Huang, X. M. Lu, W. W. Lin, Y. Kan, J. T. Zhang, Q. D. Chen, Z. Wang, L. B. Li, and J. S. Zhu, *Appl. Phys. Lett.* **97**, 222901 (2010).

<sup>16</sup>J. Wang, H. Zheng, Z. Ma, S. Praserthchoung, and M. Wuttig, *Appl. Phys. Lett.* **85**, 2574 (2004).

<sup>17</sup>C. Ederer and N. A. Spaldin, *Phys. Rev. Lett.* **95**, 257601 (2005).

<sup>18</sup>H. N. Lee, S. M. Nakhmanson, M. F. Chisholm, H. M. Christen, K. M. Rabe, and D. Vanderbilt, *Phys. Rev. Lett.* **98**, 217602 (2007).

<sup>19</sup>D. H. Kim, H. N. Lee, M. D. Biegalski, and H. M. Christen, *Appl. Phys. Lett.* **92**, 012911 (2008).

<sup>20</sup>H. J. Liu, K. Yao, P. Yang, Y. H. Du, Q. He, Y. L. Gu, X. L. Li, S. S. Wang, X. T. Zhou, and J. Wang, *Phys. Rev. B* **82**, 064108 (2010).

<sup>21</sup>X. W. Tang, J. M. Dai, X. B. Zhu, J. C. Lin, Q. Chang, D. J. Wu, W. H. Song, and Y. P. Sun, *J. Am. Ceram. Soc.* **95**, 538 (2012).

<sup>22</sup>H. Yang, H. Y. Wang, J. Yoon, Y. Q. Wang, M. Jain, D. M. Feldmann, P. C. Dowden, J. L. MacManus-Driscoll, and Q. X. Jia, *Adv. Mater.* **21**, 3794–3798 (2009).

<sup>23</sup>M. C. Martin, G. Shirane, Y. Endoh, K. Hirota, Y. Moritomo, and Y. Tokura, *Phys. Rev. B* **53**, 14285 (1996).

<sup>24</sup>S. Habouti, R. K. Shiva, C.-H. Solterbeck, and M. Es-Souni, *J. Appl. Phys.* **102**, 044113 (2007).

<sup>25</sup>R. C. O'Handley, *Modern Magnetic Materials, Principles and Applications* (Wiley, New York, 2000), pp. 437–452.

<sup>26</sup>J. W. Lu and S. Stemmer, *Appl. Phys. Lett.* **83**, 2411 (2003).

<sup>27</sup>J. Pérez de la Cruz, E. Joanni, P. M. Vilarinho, and A. L. Kholkin, *J. Appl. Phys.* **108**, 114106 (2010).

<sup>28</sup>L. Z. Cao, W. Y. Fu, S. F. Wang, Q. Wang, Z. H. Sun, H. Yang, B. L. Cheng, H. Wang, and Y. L. Zhou, *J. Phys. D: Appl. Phys.* **40**, 1460 (2007).

<sup>29</sup>A. K. Tagantsev and I. A. Stolichnov, *Appl. Phys. Lett.* **74**, 1326 (1999).

<sup>30</sup>M. D. Biegalski, D. H. Kim, S. Choudhury, L. Q. Chen, H. M. Christen, and K. Dörr, *Appl. Phys. Lett.* **98**, 142902 (2011).

<sup>31</sup>C. Wang, K. J. Jin, Z. T. Xu, L. Wang, C. Ge, H. B. Lu, H. Z. Guo, M. He, and G. Z. Yang, *Appl. Phys. Lett.* **98**, 192901 (2011).

<sup>32</sup>A. Q. Jiang, C. Wang, K. J. Jin, X. B. Liu, J. F. Scott, C. S. Hwang, T. A. Tang, H. B. Lu, and G. Z. Yang, *Adv. Mater.* **23**, 1277 (2011).